JOURNAL OF SOLID STATE CHEMISTRY 76, 87–96 (1988)

Structure and Bonding in Li_2MoO_3 and $Li_{2-x}MoO_3$ ($0 \leq x \leq 1.7$)

A. C. W. P. JAMES AND J. B. GOODENOUGH*

Center for Materials Science and Engineering, E.T.C. 5.160, University of Texas at Austin, Austin, Texas 78712

Received November 6, 1987; in revised form March 7, 1988

Li_2MoO_3 prepared by hydrogen reduction of Li_2MoO_4 was studied by X-ray and neutron diffraction. The results imply that the previous assignment of a β-Li_2SnO_3 structure to this material ($C2/c$; a = 4.97 Å, b = 8.61 Å, c = 10.10 Å, β = 99.5°) is inappropriate. Li_2MoO_3 has a novel, disordered α-$NaFeO_2$ structure ($R\bar{3}m$; a = 2.884 Å, c = 14.834 Å) with the molybdenum present as Mo_3O_{13} clusters. This structural model is consistent with the diamagnetism and low electrical conductivity of Li_2MoO_3 and accounts for certain features of the Li_2O–MoO_2 phase diagram. The presence of Mo_3O_{13} clusters in Li_2MoO_3 was confirmed by comparison of the He–I photoelectron spectra of Li_2MoO_3 and $Zn_2Mo_3O_8$; the latter compound is known from single-crystal X-ray diffraction to contain Mo_3O_{13} clusters. Oxidative extraction of up to 85% of the lithium from Li_2MoO_3 was achieved at ambient temperature with mild oxidizing agents and electrochemically. Crystallographic studies of $Li_{2-x}MoO_3$ by X-ray and neutron powder diffraction show that lithium extraction is accompanied by migration of some molybdenum ions to sites in the lattice previously occupied by lithium ions. Electrochemical delithiation of Li_2MoO_3 is kinetically slow and not fully reversible.

Introduction

Transition-metal compounds that can undergo reversible lithium insertion/extraction at ambient temperature are of great technical interest as cathode materials for secondary lithium batteries (*1*). Since the original discovery by Whittingham (*2*) that TiS_2 would intercalate lithium reversibly, research has been concentrated on transition-metal layered chalcogenides (*3*), Chevrel phases (*4*), layered oxides (*5, 6*), and framework structures such as defect spinels (*7*). As an extension of recent work on electrochemical lithium extraction from the layered oxides $LiCoO_2$ (*5*) and $LiNiO_2$ (*6*), it was decided to investigate Li_2MoO_3.

The initial decision was based on the assumption that Li_2MoO_3 had the β-Li_2SnO_3 structure and on an interest to learn whether this structure would permit lithium extraction without displacement of the transition-metal atom to the lithium layers. Several workers (*8–10*) have used X-ray powder diffraction data to assign to Li_2MoO_3 the monoclinic β-Li_2SnO_3 structure (Fig. 1). This structure consists of a cubic close-packed oxide-ion lattice with the octahedral interstices filled by cations in an ordered way: basal planes of octahedral sites alternatively contain Li^+ only and $\frac{1}{3}Li^+$, $\frac{2}{3}Sn^{4+}$. Furthermore, the Sn^{4+}-containing layers are ordered to give a continuous hexagonal network of Sn^{4+} ions. The layered $LiCoO_2$ structure, which has its layered sites alternatively Li and Co only, allows reversible electrochemical extraction of lithium with fast electrode kinetics

* To whom correspondence should be addressed.

0022-4596/88 $3.00

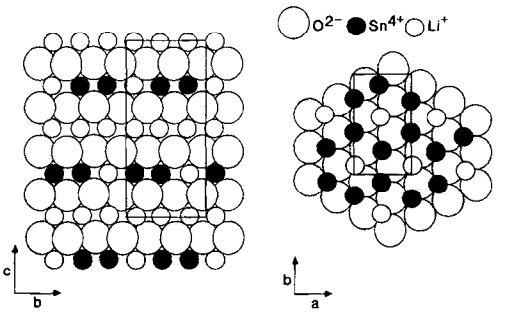

FIG. 1. The β-Li_2SnO_3 structure.

because of rapid lithium-ion diffusion within the lithium layers (*11*). Therefore, a Li_2MoO_3 phase with the β-Li_2SnO_3 structure could be expected to have similar electrode kinetics. Another reason to predict good electrode performance from such a Li_2MoO_3 phase is suggested by Fig. 2, which is a qualitative electronic energy-level diagram for Mo^{4+} (d^2) ions in a Li_2MoO_3 having the β-Li_2SnO_3 structure. The parent octahedral site allows 4*d*-electron occupancy at a $Mo^{4+}:4d^2$ ion of only two of the three t_2 orbitals. A trigonal component to the crystal field splits the manifold of three t_2 orbitals into one a_1 orbital parallel to the trigonal axis and two e_π orbitals giving strong Mo–Mo overlap in the basal plane; with two distinguishable Mo atoms per unit cell in the basal plane, orbital overlap in the Mo–Mo network splits the e_π band into separate bonding and antibonding bands. The $Mo^{4+}:4d^2$ configuration in this structure should have the bonding e_π band exactly filled; we therefore expected $Li_{2-x}MoO_3$ to be a metallic conductor in the range $0 < x < 2$. $Li_{2-x}MoO_3$ would then provide the combination of good electronic conductivity, high lithium-ion mobility (in the pure Li^+ layers of the structure) and structural stability needed for a reversible cathode in a lithium battery. Furthermore, the $Mo^{5+/4+}$ couple is sufficiently strongly oxidizing to give a useful cell voltage of over 2 V against lithium metal. Gopalakrishnan and Bhat (*10*) have recently reported that large amounts of lithium can be oxidatively extracted from Li_2MoO_3 with bromide solutions.

On the other hand, it should be noted that the Li_2MoO_3 structure described above is unexpected in view of the known solid-state chemistry of molybdenum (*12*). Generally, Mo–Mo interactions in oxides do not stabilize broad bands of extended Bloch states; Mo–Mo clusters or chains rather than metallic bonding are commonly found across shared octahedral-site edges for Mo^{5+}, Mo^{4+}, and Mo^{3+} ions. Molybdenum oxide bronzes are rare (*13*). For example, molybdenum clustering is found in the series of ternary tetravalent molybdates $M_2^{2+}Mo_3O_8$ (M = Zn, Mg, Mn, Fe, Co, Ni, Cd) (*14*). The structure of $Zn_2Mo_3O_8$ has been refined from single-crystal X-ray data (*15*) and is shown in Fig. 3. It consists of a double hexagonal closest packing (*abcb*) of oxide ions in which the oxygen layers are alternately held together by partially filled layers of octahedral and tetrahedral Zn^{2+} and three-quarter-filled close-packed layers of Mo^{4+} octahedra. Each Mo^{4+} ion shares octahedral-site edges with four neighboring Mo^{4+} ions on linear chains intersecting at 60° so as to make an array of corner-shared triangles. A cooperative dimerization along each chain results in six-electron triangular Mo_3O_{13} clusters. The Mo–Mo separation is 2.524 Å within the cluster and 3.255 Å

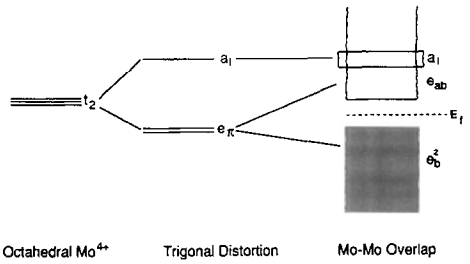

FIG. 2. Qualitative energy-level diagram for the t_2 manifold of Mo^{4+} ($4d^2$) ions in a Li_2MoO_3 having the β-Li_2SnO_3 structure.

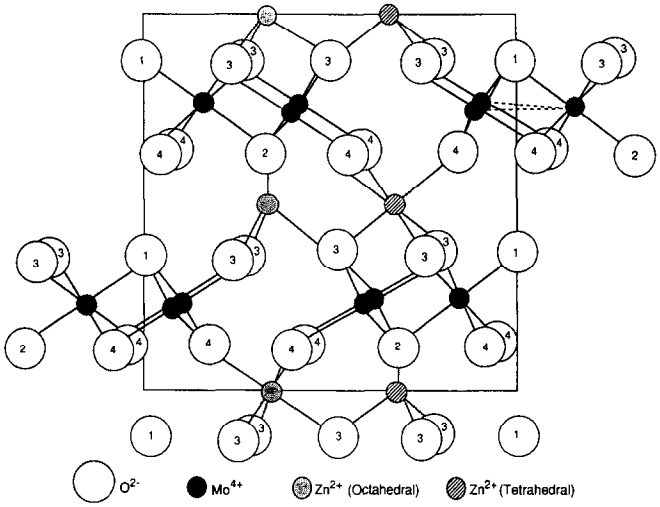

FIG. 3. The $Zn_2Mo_3O_8$ structure (after Ref. (*15*)).

between clusters. Cotton (*16*) has carried out LCAO–*MO* calculations on Mo_3O_{13} clusters; his results confirm that the clusters are strongly favored over isolated MoO_6 octahedra in the case of Mo^{4+}: the six 4*d*-electrons of Mo_3O_{13} exactly fill the a_1 and *e* bonding orbitals of the cluster. Our investigation of Li_2MoO_3, described below, demonstrates that the previously reported β-Li_2SnO_3 structure for this compound is incorrect; the stability of the Mo–Mo interactions stabilizes instead a layered structure containing Mo_3O_{13} clusters.

Experimental

Preparation of Li_2MoO_3 and $Li_{2-x}MoO_3$. Li_2MoO_3 was prepared by the method of Gleitzer (*17*). Predried MoO_3 (BDH AnalaR 99.8%) and Li_2CO_3 (BDH AnalaR 99.5%) were ground intimately and heated under a stream of dry air at 873 K for 24 hr. The resulting Li_2MoO_4 was ground and reduced in a stream of dry hydrogen at 923 K for 48 hr to give Li_2MoO_3. The product is a black, air-stable solid. The lithium and molybdenum compositions were found by atomic-absorption analysis, and the Mo^{4+} was determined by the reducing-power analysis of Choain and Marion (*18*) and confirmed by thermogravimetry in air with a Stanton-Redcroft 11/785 thermobalance. All the analyses were consistent with the composition Li_2MoO_3 to within 3%. The X-ray diffraction pattern of this material matched those given for Li_2MoO_3 in the literature (*8–10*) with no extraneous peaks. The phase prepared corresponds to the β-Li_2MoO_3 described by Réau *et al.* (*8*); we were unable to prepare the closely related α-Li_2MoO_3 that they describe.

Chemical oxidative extraction of lithium from Li_2MoO_3 was achieved by vigorous stirring of Li_2MoO_3 in solutions of Br_2 (0.05 *M* in dry acetonitrile) or I_2 (0.1 *M* in dry acetonitrile) for 7 days at ambient temperature under a reduced pressure of dry nitrogen. The extraction was done with standard Schlenk techniques, and in each case the product was analyzed by atomic-absorption analysis, Mo^{4+} reducing-power analysis and thermogravimetry in air. The product compositions found were $Li_{0.3}MoO_3$ for the bromine extraction and $Li_{0.9}MoO_3$ for the iodine extraction; both samples were free from H^+.

The samples of Li_2MoO_3 and $Li_{2-x}MoO_3$ were all found to be diamagnetic at room temperature with electrical resistivity $>10^7$ ohm cm.

Diffraction measurements. X-ray powder diffraction measurements were made on a Philips APD 3520 diffractometer. The diffractometer incorporates a Gaussian peak-fitting program for accurate location of diffraction peaks, and cell parameters were refined by a least-squares iterative method implemented on a VAX 11/785 minicomputer. Peak intensities for a given structural model were calculated with the program LAZY PULVERIX (*19*).

Powder neutron diffraction on Li_2MoO_3 and $Li_{0.9}MoO_3$ was performed on the D1A instrument at ILL Grenoble. The diffraction patterns were processed with standard Rietveld programs (*20, 21*). All diffraction measurements were made at room temperature.

Electrochemical measurements. Electrochemical extraction of lithium from Li_2MoO_3 was carried out in a test cell of the Mizushima type (*5*). Finely ground Li_2MoO_3 (about 20 mg) was pressed at 10 tons onto a 1-cm-diameter grid cut from 60-mesh stainless-steel gauze. Once pressed, the grid was assembled into the cell of Fig. 4 in an argon-filled glove box. The liquid electrolyte was a 1 *M* solution of $LiBF_4$ in purified (*22*) propylene carbonate; the lithium anode and reference electrode were separated from the cathode and each other by electrolyte-soaked Whatman glass-fiber pads. The whole assembly was compressed by screwing together the stainless-steel spigots until a stable voltage was obtained between the cathode and both the counter and the reference electrodes. Oxidative lithium extraction was carried out by galvanostatic charging at 10–20 μA. The compositional dependence of the open-circuit voltage (OCV) versus lithium was obtained by extracting the lithium stepwise (Δx = 0.1) and allowing the cell to equilibrate for 2 weeks before measuring the voltage and continuing the delithiation.

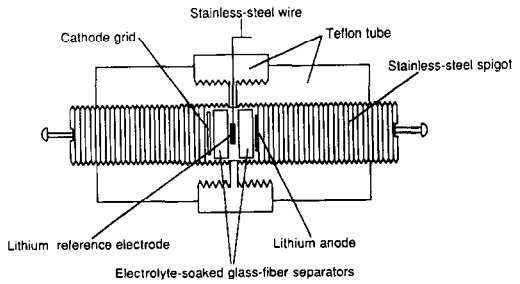

FIG. 4. Electrochemical cell for lithium cycling.

$Li_{2-x}MoO_3$ cells were charged up to x = 1.1 only; they were then discharged stepwise back to Li_2MoO_3 in order to study the reversibility of the electrochemical lithium extraction. The experiment was interfaced to a Rade microcomputer for continuous monitoring of the current and voltage.

Photoelectron spectra. In order to establish the presence of Mo_3O_{13} clusters in Li_2MoO_3, its He–I photoelectron spectrum was compared with that of $Zn_2Mo_3O_8$, which is known to contain Mo_3O_{13} clusters (*15*). $Zn_2Mo_3O_8$ was prepared by the method of McCarroll *et al.* (*14*): ZnO (Koch-Light 99.999%) and MoO_2 (Cerac 99.9%) were mixed in stoichiometric proportion and pressed into a 13-mm-diameter pellet at 10 tons pressure. The pellet was wrapped in Pt foil and heated in an evacuated silica ampoule ($p < 10^{-4}$ Torr) at 1300 K for 48 hr. The product was found by X-ray diffraction to be pure $Zn_2Mo_3O_8$ with no trace of starting material.

PES samples of Li_2MoO_3 and $Zn_2Mo_3O_8$ were pressed into 13-mm-diameter pellets at 10 tons pressure and introduced into the preparation chamber of an ESCALAB-5 electron spectrometer. Since there was some surface oxidation of Mo^{4+} to Mo^{6+} in both cases, the samples were initially reduced at 770 K under 10 Torr of hydrogen. This was followed by surface desorption at

up to 900 K under a dynamic vacuum of $<10^{-9}$ Torr. Following transfer to the main chamber, X-ray photoelectron spectra were found to be free of signals due to carbon or other contaminants. XPS of the molybdenum core levels showed that all the Mo was present as Mo^{4+}. Sample stoichiometry (except for lithium) was monitored *in situ* by measuring intensities of the dominant core peaks in XPS. The results indicate that the surface composition is close to that of the bulk material. He–I PES and HREELS spectra were obtained under a dynamic vacuum $<10^{-10}$ Torr.

Results and Discussion

Structure of Li_2MoO_3. The neutron diffraction pattern of Li_2MoO_3 is shown in Fig. 5. Both the neutron and the X-ray diffraction patterns of Li_2MoO_3 can be indexed to a trigonal unit cell ($R\bar{3}m$; $a = 2.884$ Å, $c = 14.834$ Å). Although the patterns can also be indexed to the monoclinic unit cell of the β-Li_2SnO_3 structure ($C2/c$; $a = 4.97$ Å, $b = 8.61$ Å, $c = 10.10$ Å, $\beta = 99.5°$), this indexation is unrealistic since it assumes that a number of peaks, which are predicted to be intense for this structure and which are clearly observable in the X-ray and neutron diffraction patterns of β-Li_2SnO_3 itself (*23*), are undetectably weak in the case of Li_2MoO_3. The diffraction patterns of Li_2MoO_3 closely resemble those of Li CoO_2 and $LiNiO_2$ (*24*), both of which have the layered α-$NaFeO_2$ structure shown in Fig. 6 ($R\bar{3}m$; $a = 3.025$ Å, $c = 16.094$ Å), consisting of a cubic close-packed oxide-ion lattice with basal planes of octahedral sites alternately filled with Na^+ and Fe^{3+} ions. Therefore, a new structural model was adopted as the basis for Rietveld refinement of the neutron-diffraction profile of Li_2MoO_3: the α-$NaFeO_2$ structure with Na layers replaced by Li and Fe layers replaced by a randomly distributed mixture of 1/3Li, 2/3Mo.

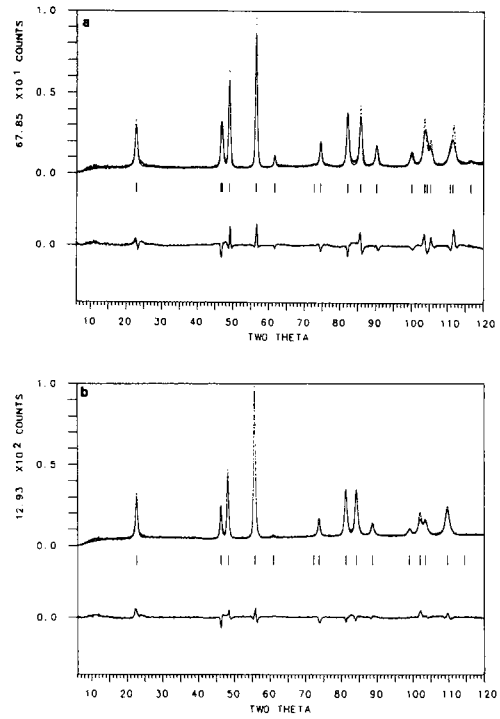

FIG. 5. Neutron-diffraction profile refinements of (a) Li_2MoO_3 and (b) $Li_{0.9}MoO_3$. Observed data as points; calculated and difference profiles as lines.

The refinement converged rapidly to the structure given in Table I; Mo and Li(1) occupancies cannot be refined simultaneously, so they were constrained according to the stoichiometry of the compound. The high R factor was due to the low neutron-beam intensity at the time the measurements were made, resulting in a low signal-to-noise ratio; the R factor expected on the basis of counting statistics is almost the same as that obtained from the refinement (Table I). The rather broad and non-Gaussian diffraction peaks also contributed to the R factor; the refinement was optimized by fitting the peaks to the Lorentzian function given in Table I. Later, repeated sintering of the sample of Li_2MoO_3 at 1150 K sharpened the diffraction peaks, but it did not otherwise alter the structure. The layered nature of the struc-

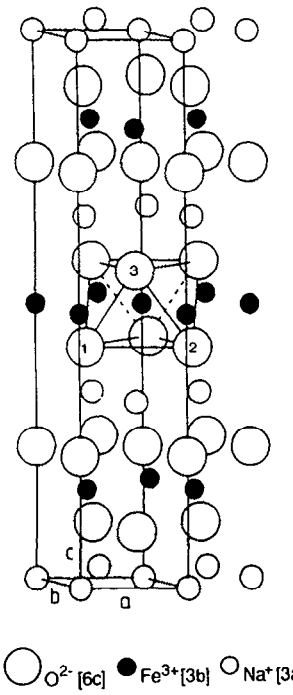

FIG. 6. The α-$NaFeO_2$ structure.

ture suggested that particle orientation effects might also be contributing to the R factor, but refinement of the preferred-orientation parameter showed that this effect is negligible. Individual atomic temperature factors could not be refined. X-ray and neutron powder-diffraction integrated peak intensities calculated from the refined structure are in excellent agreement with observed values; this is reflected in the low value of the Bragg R factor in Table I.

The diamagnetism of Li_2MoO_3 implies that the Mo^{4+} (d^2) ions are not present as isolated MoO_6 octahedra, but as randomly distributed planar clusters or chains such that each Mo makes two homopolar bonds with neighboring Mo ions. As discussed above, this condition is most easily fulfilled by formation of Mo_3O_{13} triangular clusters. (The alternative—formation of zigzag Mo chains—is observed in β-$MoTe_2$ and cannot be ruled out here; however, it should be noted that the end members of such a chain will be paramagnetic, so the chains in Li_2MoO_3 would have to be very long to account for the observed diamagnetism.) If we assume that the Mo is present as Mo_3O_{13} clusters, then the disordered structure of Li_2MoO_3 is readily accounted for: the very low mobility of Mo locked into Mo_3O_{13} clusters prevents rearrangement of the clusters into ordered arrays at the moderate temperatures employed to make Li_2MoO_3.

TABLE I

STRUCTURAL PARAMETERS OF Li_2MoO_3 AND $Li_{0.9}MoO_3$

Atom	Position	x/a	y/b	z/c	Occupancy
	Li_2Mo: Space group $R\bar{3}m$; $a = b = 2.884(0.001)$ Å, $c = 14.834(0.002)$ Å				
Mo	3b	0.00	0.00	0.500	0.333(0.002)
Li(1)	3b	0.00	0.00	0.00	0.167(0.002)
Li(2)	3a	0.00	0.00	0.00	0.500(0.002)
O	6c	0.00	0.00	0.246(0.000)	1.000(0.001)
	$Li_{0.9}MoO_3$: Space group $R\bar{3}m$; $a = b = 2.906(0.001)$ Å, $c = 14.904(0.002)$ Å				
Mo(1)	3b	0.00	0.00	0.50	0.270(0.002)
Mo(2)	3a	0.00	0.00	0.00	0.063(0.002)
Li(1)	3b	0.00	0.00	0.50	0.002(0.002)
Li(2)	3a	0.00	0.00	0.00	0.300(0.002)
O	6c	0.00	0.00	0.243(0.000)	1.000(0.001)

Note. Standard deviations of refinable parameters given in parentheses. For Li_2Mo, overall isotropic temperature factor, $B_{iso} = 0.61(0.06)$ Å^2. $R_p = 11.3\%$, $R_{wp} = 14.5\%$, $R_b = 4.9\%$, R_{wp}(expected) = 14.0%. For $Li_{0.9}MoO_3$, overall isotropic temperature factor, $B_{iso} = 2.03(0.06)$ Å^2. $R_p = 6.7\%$, $R_{wp} = 9.6\%$, $R_b = 3.2\%$, R_{wp}(expected) = 10.1%).

$$R_p = 100\,\frac{\Sigma|Y_{obs} - Y_{calc}|}{\Sigma Y_{obs}}, \quad R_{wp} = 100\left(\frac{\Sigma w_i|Y_{obs} - Y_{calc}|^2}{\Sigma w_i Y_{obs}^2}\right)^{1/2},$$

$$R_b = 100\,\frac{\Sigma|I_{obs} - I_{calc}|}{\Sigma I_{obs}},$$

$$R_{wp}(\text{expected}) = 100\left(\frac{(N - P + C)}{\Sigma w_i Y_{obs}^2}\right)^{1/2},$$

where I = integrated Bragg intensity, Y = number of counts at angle 2θ, w_i = weighting factor for the ith data point, N = number of statistically independent observations, P = number of least-squares parameters in the refinement, C = number of constraint functions in the refinement. The Lorentzian peak shape function employed in the refinement is given by

$$I_i/I_K = \frac{2\sqrt{C}}{\pi H_K}\,\frac{H_K^2}{[1 + C(2\theta_i - 2\theta_K)^2]^2},$$

where H_K = full width at half maximum of the Kth peak (refinable parameter), $C = 4(\sqrt{2} - 1)$, $2\theta_K = 2\theta$ position of the Kth reflection.

The other phases in the Li_2O–MoO_2 system probably have similar structures. Réau *et al.* (*8*) reported phases $Li_6Mo_2O_7$ and $Li_4Mo_5O_{12}$, both with X-ray diffraction patterns very similar to that of Li_2MoO_3. These phases and Li_2MoO_3 form a continuous solid solution above 1100°C. The disordered nature of the Li_2MoO_3 structure enables the Li : Mo ratio in these compounds to vary over a wide range without a change of structural type.

Structure of $Li_{2-x}MoO_3$. The X-ray and neutron diffraction patterns of $Li_{0.9}MoO_3$ resemble those of Li_2MoO_3 and can be indexed to a nearly identical trigonal unit cell ($R\bar{3}m$; a = 2.906 Å, c = 14.904 Å); this implies that no phase change takes place on delithiation. However, Rietveld refinement of the neutron-diffraction profile (carried out as described above for Li_2MoO_3) demonstrates that the delithiation is not topotactic; the refinement converges rapidly to the structure given in Table I, in which nearly 20% of the molybdenum atoms, along with all the lithium ions formerly in the molybdenum-containing layers, have migrated into the layers of octahedral sites formerly occupied by lithium only. This displacement of Mo ions can be explained as follows: oxidation of Mo_3O_{13} clusters is followed by disproportionation of the oxidized clusters to give isolated octahedral Mo^{6+} ions that migrate to electrostatically favored sites vacated by lithium in the alternate layers. Molybdenum displacement also accounts for the fact that the *c*/*a* lattice parameter ratio in $Li_{0.9}MoO_3$ is 0.5% less than that in Li_2MoO_3; if the lithium extraction were topotactic, then the *c*/*a* ratio would be expected to increase as the lithium is removed because of increased electrostatic repulsion between close-packed oxide-ion layers; for example, the *c*/*a* lattice parameter ratio of $Li_{0.5}CoO_2$ prepared by topotactic lithium extraction from Li CoO_2 is 2% greater than that of $LiCoO_2$ itself (*24*) (Figs. 7a and 7b). In the case of

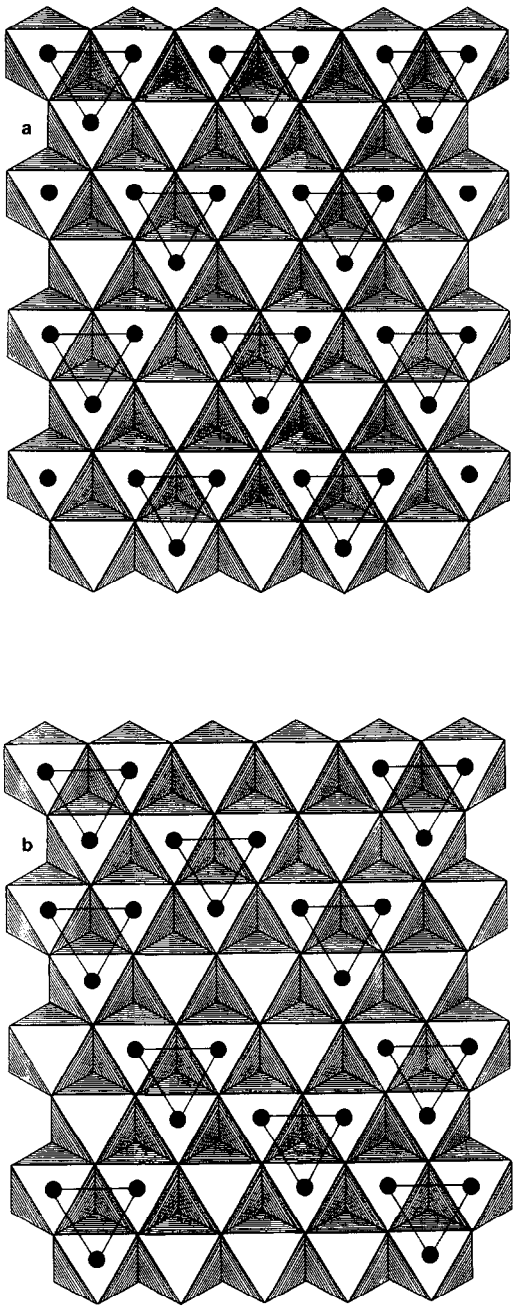

FIG. 7. Distribution of molybdenum ions in close-packed layers: (a) three-fourths of sites in layer occupied by Mo^{4+}; ordered array of Mo_3 clusters found in $Zn_2Mo_3O_8$. (b) Two-thirds of sites in layer occupied by Mo^{4+}; random distribution of Mo_3 clusters found in Li_2MoO_3.

$Li_{0.9}MoO_3$, the lithium-depleted layers are held together by the displaced Mo^{6+}; this is also reflected in the small shift in the relative positions of the oxide–ion layers. Finally, we note that the overall isotropic temperature factor (individual atomic temperature factors cannot be refined) is too high to be accounted for by thermal vibrations alone; it must be due to small, random variations in atomic positions arising from the disordered nature of the delithiated structure and the formation of molybdenum(VI)–oxygen double bonds.

A similar displacement of transition-metal ions to that in $Li_{2-x}MoO_3$ has been observed in the delithiation of the layered vanadate $LiVO_2$ (*27*), which has the α-Na FeO_2 structure. In this case, oxidative extraction of Li leads to migration of vanadium ions into layers formerly occupied by lithium only. Such migrations are undesirable in lithium-battery cathode materials because the displaced transition-metal ions reduce the lithium-ion mobility and because the displacement is generally irreversible.

The X-ray diffraction pattern of $Li_{0.3}MoO_3$ shows it to be virtually amorphous; the processes of disproportionation and migration of molybdenum have completely disrupted the original Li_2MoO_3 structure.

Electrical measurements. Figure 8 shows the compositional variation of the OCV versus lithium metal for $Li_{2-x}MoO_3$ ($0 \leq x \leq 1.1$). Data for both charging and discharging of a 19-mg sample of Li_2MoO_3 are shown. The irreversibility of the electrochemical delithiation is apparent after just one charge–discharge cycle; it rules out $Li_{2-x}MoO_3$ as a reversible cathode for lithium secondary batteries. The OCV of Li_2MoO_3 itself (2.3 V) is higher than that of MoO_2 (1.7 V) (*25*). This difference implies that the Fermi level is lower-lying in Li_2MoO_3, where the Mo^{4+} *d*-electrons are localized in clusters, than in metallic MoO_2; Mo–Mo dimerization in MoO_2 places the Fermi level in a partially filled π^* band that

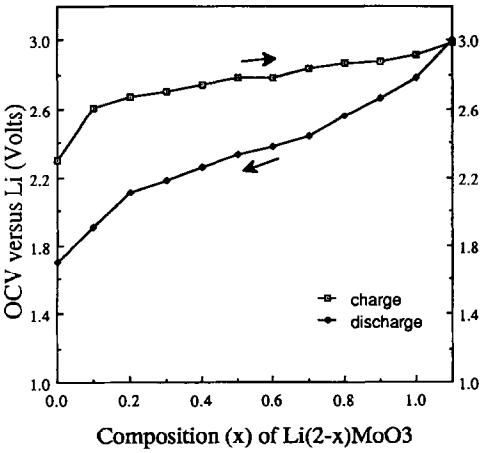

FIG. 8. Open-circuit voltage versus composition for a single charge–discharge cycle of $Li_{2-x}MoO_3$ ($0 < x < 1.1$).

is antibonding with respect to Mo–O π bonding and nonbonding with respect to Mo–Mo interactions (*26*). PES measurements place the π^* band approximately 1 eV above the Mo–Mo bonding state in MoO_2 (*26*). The impedance of the $Li_{2-x}MoO_3$ cell was extremely high; the electronic impedance was several thousand ohms and lithium-ion diffusion within the electrode was slow. The slow diffusion meant that the cell took 2 weeks to equilibrate on open circuit before the OCV could be measured for a given composition.

Photoelectron spectroscopy. The He–I photoelectron spectra of Li_2MoO_3 and $Zn_2Mo_3O_8$ are shown in Fig. 9; the binding energies are referred to the Fermi energy. The photoelectrons with binding energy <3.6 eV arise from ionization of Mo^{4+} 4*d* levels, the intense signal between 3.6 and 10 eV is due to ionization of the oxygen 2*p* manifold, and the peaks at higher binding energy (lower photoelectron kinetic energy) are due to secondary electrons.

The photoelectron spectrum of $Zn_2Mo_3O_8$ in the Mo 4*d* region consists of two overlapping Gaussian peaks. This spectrum can be rationalized as follows: according to

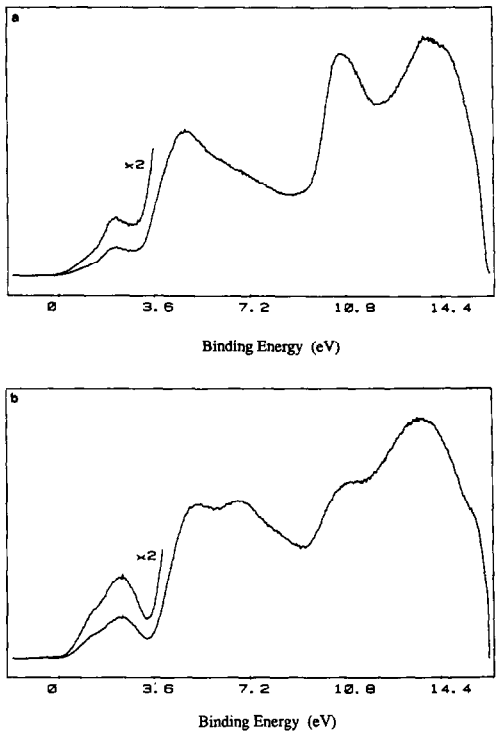

FIG. 9. He–I photoelectron spectra of (a) Li_2MoO_3 and (b) $Zn_2Mo_3O_8$.

Cotton (*16*), the six Mo 4*d*-electrons in the Mo_3O_{13} clusters of $Zn_2Mo_3O_8$ occupy the a_1 lowest bonding orbital and the next-lowest *e* degenerate pair of bonding orbitals; hence two distinct PES peaks are expected. The close similarity of the Li_2MoO_3 photoelectron spectrum to that of $Zn_2Mo_3O_8$ in the Mo 4*d* region is strong evidence for Mo_3O_{13} clusters within the disordered $LiMo_2$ layers of Li_2MoO_3. In particular, there is no significant broadening of the 4*d* ionization band in Li_2MoO_3 such as would be expected if the Mo was forming larger clusters of chains, and there is no sign of a Fermi edge (or the plasmon mode in EELS) that would be expected if the Mo was engaged in metallic bonding.

Proof of the structural model proposed for Li_2MoO_3 must await the preparation of single crystals for X-ray diffraction. The refractory nature and disordered structure of Li_2MoO_3 make it hard to grow large single crystals, but this might be possible, for example, by slow electrolysis of Li_2MoO_4 (mp 649 °C).

References

1. J.-P. GABANO, "Lithium Batteries," Academic Press, New York (1983).
2. M. S. WHITTINGHAM, *Mater. Res. Bull.* **9,** 1681 (1974).
3. M. S. WHITTINGHAM, *Prog. Solid State Chem.* **12,** 41 (1978).
4. R. SCHOELLHORN, M. KÜMPERS, AND J. O. BESENHARD, *Mater. Res. Bull.* **12,** 781 (1977).
5. K. MIZUSHIMA, P. C. JONES, P. J. WISEMAN, AND J. B. GOODENOUGH, *Mater. Res. Bull.* **15,** 783 (1980).
6. M. G. S. R. THOMAS, W. I. F. DAVID, AND J. B. GOODENOUGH, *Mater. Res. Bull.* **20,** 1137 (1985).
7. J. B. GOODENOUGH, M. M. THACKERAY, W. I. F. DAVID, AND P. G. BRUCE, *Rev. Chim. Miner.* **21,** 435 (1984).
8. J.-M. RÉAU, C. FOUASSIER, AND C. GLEITZER, *Bull. Soc. Chim. Fr.* **1967,** 4294 (1967).
9. G. LANG, *Z. Anorg. Allg. Chem.* **348,** 246 (1966).
10. J. GOPALAKRISHNAN AND V. BHAT, *Mater. Res. Bull.* **22,** 769 (1987).
11. M. G. S. R. THOMAS, P. G. BRUCE, AND J. B. GOODENOUGH, *Solid State Ionics* **17,** 13 (1985).
12. J. B. GOODENOUGH, *in* "Chemistry and Uses of Molybdenum," Climax Chemical Co. (1984).
13. A. WOLD, W. KUNNMANN, R. J. ARNOTT, AND A. FERRETTI, *Inorg. Chem.* **3,** 545 (1963).
14. W. H. MCCARROLL, L. KATZ, AND R. WARD, *J. Amer. Chem. Soc.* **79,** 5410 (1957).
15. G. B. ANSELL AND L. KATZ, *Acta Crystallogr.* **21,** 482 (1966).
16. F. A. COTTON, *Inorg. Chem.* **3,** 1217 (1964).
17. C. GLEITZER, *Bull. Soc. Chim. Fr.* **1966,** 1913 (1966).
18. C. CHOAIN AND F. MARION, *Bull. Soc. Chim. Fr.* **1963,** 212 (1963).
19. K. YVON, W. JEITSCHKO, AND E. PARTHE, *J. Appl. Crystallogr.* **10,** 73 (1977).
20. H. M. RIETVELD, *J. Appl. Crystallogr.* **2,** 65 (1969).
21. A. W. HEWAT, NBS Spec. Publ. (US), 567, 111-41 (1980).
22. R. JASINSKI, *Adv. Electrochem. Electrochem. Eng.* **8,** 253 (1971).
23. J. L. HODEAU, M. MAREZIO, A. SANTORO, AND R. S. ROTH, *J. Solid State Chem.* **45,** 170 (1982).

24. M. G. S. R. THOMAS, Ph.D. Thesis, Oxford (1985).
25. D. W. MURPHY, F. J. DISALVO, J. N. CARIDES, AND J. V. WASZCZAK, *Mater. Res. Bull.* **13,** 1400 (1978).
26. N. BEATHAM AND A. F. ORCHARD, *J. Electron. Spectrosc. Relat. Phenom.* **16,** 77 (1979).
27. M. M. THACKERAY, L. A. DE PICCIOTTO, W. I. F. DAVID, P. G. BRUCE, AND J. B. GOODENOUGH, *J. Solid State Chem.* **67,** 285 (1987).